Supplementary material

Supplementary material for manuscript “Sub 20 nm metal-conjugated molecule junctions acting as a nitrogen dioxide sensor ”

Contents

Supplementary material for manuscript “Interactions between conjugated molecules and nitrogen dioxide as probed using sub 20 nm molecular chemiresistor” 1
1- Materials and methods 2
1.1. Gold nanoelectrodes 2
1.2. Protected gold nanoparticles 2
1.3. Trapping of protected gold nanoparticles in the nanogaps 3
1.4. Electrical characterization 3
1.5. Theoretical calculations 3
1.6. Gas sensing; 4
1.7. Fabrication and understanding of molecular chemiresistor with 4,4'biphenyldithiol (BPDT).4
2- Exposure of the molecular nanodevice to nitrogen dioxide 6
3- Measurement of binding energy and sticking probability.....6
4- Control experiment and theory.....9
5- References.....9
6- Figures 11

1- Materials and methods

The molecular nano-device housed on Si/SiO_2 substrate is fabricated in three stages as illustrated in Schematic S1 and realization of this scheme is shown in experimental **Fel! Hittar inte referenskälla.**.

1.1. Gold nanoelectrodes

Fabrication of gold nanoelectrodes was carried out as described Blom, T. et al(1) First, on a clean Si/SiO_2 substrate with oxide layer thickness of ≈300nm, electron beam lithography was performed to fabricate thin wires of gold. Environmental scanning electron microscope (ESEM, XL-30) at acceleration voltage of 30kV was used for this purpose. Approximately 150nm thick layer of PMMA was spin coated on the substrate and nanoelectrode designs which are 130µm long and ≈200nm wide in the middle, were patterned and then subsequently developed in 1:3||MIBK:IPA. Second, Metal deposition was carried out by physical vapor deposition technique using Lesker PVD-75 apparatus. At first a ≈ 3 nm layer of titanium was deposited using e-beam evaporation and then 65 nm layer of gold was deposited by resistive evaporation technique. Titanium layer served the purpose of adhesion layer between gold and silicon dioxide. Metal lift off was done by soaking the wafer in acetone for 5 hours and subsequently sonication and rinsing with IPA. After this contact pads were fabricated on the ends of the gold lines with, gold. Photolithography was done for this purpose. Photoresist was deposited by spin coating and exposure was done through photolithographic mask which was customized to design of the EBL patterns. Approximately 3nm titanium and 150nm gold was deposited using PVD and metal lift-off was done as described in above lines. Finally nanogaps were cut using focused beam of Gallium ions. We used FEI Strata DB235 FIB / SEM / EDS / Cryo instrument for milling nanogaps. FIB was aligned at 30keV energy and 1pA current. A fine line was milled in the middle of the individual EBL wires which resulted in nanogap whose size was ≈20nm as observed in scanning electron microscope image of Figure S 1(a). We used LEO-1550 (Zeiss) operated at 15 kV for SEM observation.

1.2. Protected gold nanoparticles

Protected AuNPs i.e. ω-thiol protected α,ω-octane dithiol coated gold nanoparticles were prepared by wet chemistry as demonstrated earlier.(2) These AuNPs were used as

suspension in toluene. Figure S 1(c) shows SEM image of the gold nanoparticles. For SEM imaging the AuNPs were supported on Si/SiO2 substrate by drop casting.

1.3. Trapping of protected gold nanoparticles in the nanogaps

Nanoparticles were trapped in the nanogaps via dielectrophoretic trapping technique.(*3*) Electrical signal for producing dielectrophoretic force was generated using UTG 2062a arbitrary waveform generator. At first 8-10 µl drop of protected-AuNPs suspension was put on nanoelectrodes sample and then AC signal of 1-2V_{p-p} amplitude and 1MHz frequency was applied for about 45-60 seconds. After this the electrical connections were removed and the sample was rinsed with DI water and then blow dried with N_2 gas. After this electrical characterization i.e. two way current-voltage sweep (I-V sweep) was performed between ±300 mV bias voltage range to observe the trapping effect. Low bias resistance of the trapped nanogaps was observed to be 2 to 4 orders of magnitude smaller as compared to empty nanogaps. Electrical characterization during making of the nanodevice was done using Agilent b1500a semiconductor parameter analyzer. SEM image in Figure S 1(d) shows trapped nanoparticles in the gap.

1.4. Electrical characterization

Electrical characterization was done during fabrication of the nanoMED and during gas sensing. Two way current voltage (I-V) sweep measurements were performed with the help of Agilent b1500a semiconductor parameter analyzer (whose probe station was housed inside Faraday cage) after (i) nanogaps cutting (ii) trapping protected gold nanoparticles (iii) after molecular place exchange by BPDT. Fixed voltage bias measurements were performed during gas sensing to acquire current versus time data. Keithley 6430 sub femto amp source meter connected to custom made gas sensing chamber was used for this purpose.

1.5. Theoretical calculations

Transport calculations were carried out from first principles with a method based on nonequilibrium Green's functions (NEGF) combined with DFT as implemented in the TranSIESTA package Siesta.(*4, 5*) The relaxed molecular structures were inserted as their dithiolates between two reconstructed Au[100] surfaces and relaxed once more to optimize the Au–S bonding. The device consists of three parts: left electrode, molecule, and right electrode. The electrodes are modeled by six layers of gold atoms where the three outer

layers are relaxed, while the others are kept at the experimental bulk positions. In the lateral dimension a 6 × 6 supercell (17.5 Å × 17.5 Å) was used, large enough to remove interactions between periodic images. All relaxations are performed at the DFT level with the SIESTA package(*6*) and core electrons are modeled using Troullier-Martins(*7*) soft norm-conserving pseudopotentials. The valence electrons are expanded in a basis set of local orbitals using a double-ζ plus polarization orbital (DZP) set for electrons in the molecule and a single-ζ plus polarization orbital (SZP) for electrons in the gold electrode. The GGA was used for the exchange-correlation functional.(*8*)

1.6. Gas sensing;

To record the electrical response of the nanodevice in different gaseous environments, we used custom made gas sensor chamber which is housed inside Faraday cage and whole assembly is inside fumehood. This chamber is coupled to mass flow controllers (Brooks 5878) which can regulate the speed of different gases flowing into the chamber. To record the electrical response of the sensor nanodevice to various gas environments, the device was placed inside a custom made chamber which has provision for inserting electrical probe needles. We used Keithley 6430 sub-femto amp source meter. Light from Ocean optics DH-2000, UV-Vis-IR source is also coupled to the chamber via optical fiber. This source has Deuterium as well as Halogen lamps. For the recovery of the baseline resistance of the nanodevice we illuminated the device with UV-light using deuterium source.

1.7. Fabrication and understanding of molecular chemiresistor with 4,4'biphenyldithiol (BPDT)

EBL lines were metallized with 99.99 % gold partially because gold is suitable for creating bonds with thiols. Figure S 1(a) shows SEM image which reveals the size of the nanogap to be < 20 nm. The Figure S 1(b) shows IV characterization result of the empty nanogap. Calculated inverse slope of the linear fit gives resistance greater than 530 Tera Ohms. The ultra-high electrical resistance confirms the cleanliness of the gap and its suitability to host and electrically characterize high resistance molecules. This gap serves as the locality where molecular resistor is fabricated. The molecular nanodevice which is bridged with gold nanoparticles is shown in Figure S 1(d). The protected-AuNPs are trapped using dielectrophoretric trapping technique. Ac field is responsible for creation of

dielectrophoretic force whice which acts on the p-AuNPs and since the polarizability of toluene is different (less) than the nanoparticles, the AuNPs move towards area of higher electrical field. The electrical field is strongest near the edges of the electrodes in the nanogap hence p-AuNPs move towards the nanogap. Here emphasis should be given to the cleanliness of the sample surface before trapping step. For cleaning, sample surface is treated with UV/Ozone plasma for 30 minutes followed by immersing the sample in 99.9% ethanol to remove gold oxide. The SEM image is obtained after finishing the device characterization and gas sensing steps.

Electrical characterization is performed at each stage of synthesis and Figure S 1(e) compares two-way IV sweep results after stage 2 and stage 3. Semi log plots of current vs voltage show the characteristic current conducted by the nanodevice at different stages during the synthesis process i.e. (Stage 1) Empty gap can conduct current on the order of sub 10 femto amps whereas after (stage 2) trapping AuNPs in the gap, effective tunneling distance for electrons is reduced and nanodevice starts conducting slightly more current as compared to the empty gap i.e. on the order of 100s of femto amps. The trityl umbrella which protects ω-thiols of α,ω-ODT ligands attached to the gold nanoparticles, isolates protected-AuNPs from each other and from electrodes as it hinders the chemical linking between ω-thiol and adjacent gold surface. These ligands create inter-AuNP and AuNP-electrode distances hence current after trapping step remains limited to 1 pA at this bias. The spread of the histogram in Figure S 1(f) left panel, is caused by different configurations existing in the trapped nanodevice as described by S.H.M Jafri et al(*3*). After trapping, the devices are immersed in 10 mM solution of 4,4'-biphenyldithiol in toluene for ligand exchange reaction.(*9, 10*) This reaction takes place inside a three neck flask where argon is constantly bubbling through the solution. Argon creates inert atmosphere inside the flask to ensure that no side reactions is happening. After Place exchange of protected- ODT ligands in BPDT solution (Stage 3) there is a drop in electrical resistance of the nanodevice. This observation is partially because after ligand exchange there is chemical link (chemisorbed junctions) between the molecules and AuNPs. Gold-sulfur bonds are created and inter particle distances are reduced. Now AuNPs are bridged with π-conjugated bi-phenyl(s) which possesses delocalized electrons. This reduces the tunneling distance and potential barrier and hence more than 2 orders of magnitude increase in conduction is observed. In Figure S

1(f) right panel histograms compare the low bias resistance of devices fabricated for current work. Resistance shift of more than 2 orders of magnitude, showing drop in resistance, moving from stage 2 to stage 3, is a consequence of ligand exchange.

2- Exposure of the molecular nanodevice to nitrogen dioxide

After performing place exchange of protected ODT ligands with BPDT molecules i.e. at stage 3, modulation of conductivity is observed and all devices show change in current upon exposure to 100 ppm NO_2/N_2 as shown in Figure S 2(a-f). Values of different parameters extracted from experimental data of figure 1(A) reproduced in Figure S 2(D) are. *Base-line Current* (I_{N_2}); the mean current conducted by the device in N_2 atmosphere prior to NO_2 exposure is 15.8 pA. *Equilibrium current in nitrogen dioxide* (I_{NO_2}); the average current level maintained by the device in NO_2 for time period equal to or greater than response time is 25.9 pico Amperes. *Response time*; it has two values (a) the time taken by the current conducted by the device to change more than 10% of base line current and (b) the time taken by the device to reach 90% of its equilibrium current value. Here a = 3.5 minutes and b = 117 minutes gives total response time of 120.5 minutes. The *percentage response* R is calculated by using the formula $R = 100 \times [(I_{NO_2} - I_{N_2})/(I_{N_2})]$. For this device response is 63.9 %. Recovery time is time taken by the device to reach base-line current. It is measured between the instant when NO_2 flow is stopped and UV light illumination is started, to the time when device reaches the baseline current $(I_{N_2})\cdot$ Recovery times for different devices vary between 20 and 30 minutes. We also note here that the recovery is stimulated with UV illumination otherwise the natural recovery times measured for these devices are of the order of many hours.

3- Measurement of binding energy and sticking probability

To analyze the sensing property of molecular chemiresistor systematically, current-time measurements are performed at different concentrations of NO_2. Figure S 3(A) shows the dynamical response of the device which rises with increasing concentration of NO_2. Experimental data are obtained for NO_2 concentrations between 100 to 1500 ppb at a

constant flow rate of 150 ml/min. Following a similar procedure as explained by Winadda et al.,(*11*) the Langmuir isotherm is used to describe the adsorption of NO_2 on molecular chemiresistor. Here, the applicability of the Langmuir model might be limited since the molecule-AuNP be are a non-planar system, in a similar way as the carbon nanotubes used in references (*11, 12*) are non-planar. As one justification for the use of the Langmuir model, reference (*11*) demonstrates that the relationship between pressure P and sensor response R follows the relation:

$$\frac{P}{R} = \frac{P}{R_{max}} + \frac{1}{KR_{max}} \qquad \text{.....1}$$

Here P is partial pressure of NO_2 gas, R_{max} is the response of the device at equilibrium when $P \to \infty$ and K is the equilibrium constant. K is defined as $K = \frac{K_{ads}}{K_{des}}$ where K_{ads} is adsorption rate constant and K_{des} is desorption rate constant. R_∞ is the response of the device at equilibrium and for a pressure P. In the Figure S 3(B), it can be observed that for our measurements, P and R equally follow the evolution given by equation .....1 which suggests that the kinetics gas sensor follow Langmuir Isotherm. Here, the data points in Figure S 3(C) (blue dots) are obtained from the maximum values of the exponentials used for fitting the curves in Figure S 3(A). From the fit, values of R_{max} and K are calculated to be 0.1923 and 51.99 Pa^{-1} respectively.

The sticking probability and binding energy of NO_2 with the molecules in the nano-device is calculated as follows. The dynamics of the sticking and desorption process can be described as (*11*):

$$R(t) = R_\infty\left(1 - e^{\left(\frac{-R_{max}K_{ads}P}{R_\infty}\right)t}\right) \qquad \text{.....2}$$

Equation …….2 is fitted to the experimental curve for P=0.1ppm in Figure S 3(C), and K_{ads} is obtained as K_{ads}=4.13 $S^{-1}Pa^{-1}$. The sticking probability s_o is related to adsorption rate constant K_{ads} and the molecular flux j as $K_{ads} = s_o \times J$ which implies, the adsorption rate K_{ads} can be expressed as :

$$K_{ads} = s_o\left(\frac{\sigma}{\sqrt{2\pi k_b m T}}\right) \qquad \text{…….3}$$

Where s_o is sticking probability and σ is the molecular cross section. Using the values of K_{ads} , $(Q)_{NO_2} = 10^{-19} m^2$, Boltzmann constant $k_B = 1.3806\times10^{-23} m^2 kg s^{-2} K^{-1}$, $m_{no_2} = 7.64\times10^{-26}$ kg, and $T = 293\ K$, the sticking probability is calculated to be s_0=1.83×10^{-3} . The binding energy E_b is calculated from reference (*11*):

$$E_b = -k_B T \ln\left(\frac{K_{ads}}{\nu K}\right) \qquad \text{…….4}$$

Where k_B is Boltzmann constant K_b= 8.62 × 10^{-5}eV, ν is the attempt frequency. The attempt frequency is given in references as ν= 10^{12}-10^{14} s^{-1}.(*11-13*) One obtains E_b = 0.829 -0.888 eV. This value is very small then the theoretically calculated values of either physisorption or chemisorption which is 2.04eV and 1.04eV respectively.

Other important parameters of a sensor are its sensitivity and detection limit. Figure 3(C) shows the concentration versus response relationship for the experimental data of figure 3(B) in terms of percentage response. The slope of the linear fit to the experimental data gives a sensitivity or change of response of ΔR =13% per ppm. The detection limit P_{limit} of the sensor system is the smallest quantity of an analyte which can produce a response R of at least 3 times the relative noise of the electrical current and is thus:(*14*)

$$P_{limit} = 3 \times \frac{Noise_{rms}}{Sensitivity}.$$

By calculation the noise from the standard deviation of the baseline of the sensor response in figure 3(B), one obtains 0.002373 and P_{limit}=54.7 ppb for this chemiresistive molecular electronics device.

4- Control experiment and theory

To provide evidence that the nanoMED devices containing BPDT is only responsible for measured response to NO_2 gas molecules, we performed control experiment and theoretical calculations. For this purpose nanoMED device at stage 2 was exposed to NO_2 environment. Results shown in Figure S 4 clearly demonstrate that no change in conduction happens. This measurement was performed at 300mV applied voltage bias and under 100ppm NO_2 exposure. Measurements were also performed at different bias voltage conditions which showed no change in conductivity. So it is concluded that protected-AuNPs in between nanoelectrodes do not contribute to measured response. Since octanedithiol (ODT) molecules are in the nanoMED it is also worthwhile to investigate if they contribute to measured response. For the purpose of knowing this, theoretical calculations were performed on alkane molecule bridging the electrodes as shown in Figure S 5. This study confirms that ODT did not contribute to measured response which is rise of conduction. Figure S 5(A) shows the system with NO_2 gas molecule. NO_2 gas in the lowest energy configuration does not chemically bind to the molecule and the absorption energy is 0.60 eV. Transmission curve calculated with and without gas molecule in Figure S 5(B) clearly indicates that the transmission near fermi energy is unaffected in presence of this gas. Very small peak at Fermi level is because of the presence of NO_2. Nearly double transmission value in HOMO level indicates slight stretching in alkene chain in presence of NO_2 gas. Because of stretching and overlapping with NO_2 HOMO the peaks are slightly shifted and transmission is higher in this region, which, however, does not affect current at the low bias encountered between neighboring nanoparticles. Reported transmission spectra are in good agreement with previously reported transmission for alkanedithiol in gold electrodes.(*3*)

Finally, we can conclude from the transmission curve that alkanedithiol is not taking part in gas sensing, which is in agreement with experimental conclusion.

5- References

1. T. Blom, K. Welch, M. Strømme, E. Coronel, K. Leifer, Fabrication and characterization of highly reproducible, high resistance nanogaps made by focused ion beam milling. *Nanotechnology* **18**, 285301 (2007).
2. A. Wallner *et al.*, Formation and NMR spectroscopy of omega-thiol protected alpha,omega-alkanedithiol-coated gold nanoparticles and their usage in molecular charge transport junctions. *Langmuir* **27**, 9057-9067 (2011).
3. S. H. M. Jafri *et al.*, Nano-fabrication of molecular electronic junctions by targeted modification of metal-molecule bonds. *Scientific Reports* **5**, 14431-14431 (2015).
4. A. R. Rocha *et al.*, Spin and molecular electronics in atomically generated orbital landscapes. *Physical Review B* **73**, (2006).
5. M. Brandbyge, J.-L. Mozos, P. Ordejón, J. Taylor, K. Stokbro, Density-functional method for nonequilibrium electron transport. *Physical Review B* **65**, (2002).
6. E. e. a. Artacho, The SIESTA method; developments and applicability. *J. phys. Condens. Matter* **20**, (2008).
7. N. Troullier, J. L. Martins, Efficient pseudopotentials for plane-wave calculations. *Physical Review B* **43**, 1993-2006 (1991).
8. John P. Perdew, Kieron Burke, M. Ernzerhof, Generalized Gradient Approximation Made Simple. **77**, (1996).
9. J. Liao *et al.*, Ordered nanoparticle arrays interconnected by molecular linkers: electronic and optoelectronic properties. *Chem. Soc. Rev.* **44**, 999-1014 (2015).
10. L. Bernard *et al.*, Spectroscopy of Molecular Junction Networks Obtained by Place Exchange in 2D Nanoparticle Arrays. *The Journal of Physical Chemistry C* **111**, 18445-18450 (2007).
11. W. Wongwiriyapan, S. Inoue, S.-i. Honda, M. Katayama, Adsorption Kinetics of NO_2 on Single-Walled Carbon Nanotube Thin-Film Sensor. *Japanese Journal of Applied Physics* **47**, 8145-8147 (2008).
12. Pengfei Qi *et al.*, Toward Large Arrays of Multiplex Functionalized Carbon Nanotube Sensors for Highly Sensitive and Selective Molecular Detection. **3**, 347-351 (2003).
13. Y. Hajati *et al.*, Improved gas sensing activity in structurally defected bilayer graphene. *Nanotechnology* **23**, 505501 (2012).
14. Jing Li *et al.*, Carbon Nanotube Sensors for Gas and Organic Vapor Detection. *Nano Lett* **3**, 929-933 (2003).
15. S. H. M. Jafri *et al.*, Assessment of a nanoparticle bridge platform for molecular electronics measurements. *Nanotechnology* **21**, 435204-435204 (2010).

6- Figures

1- Schematic S1

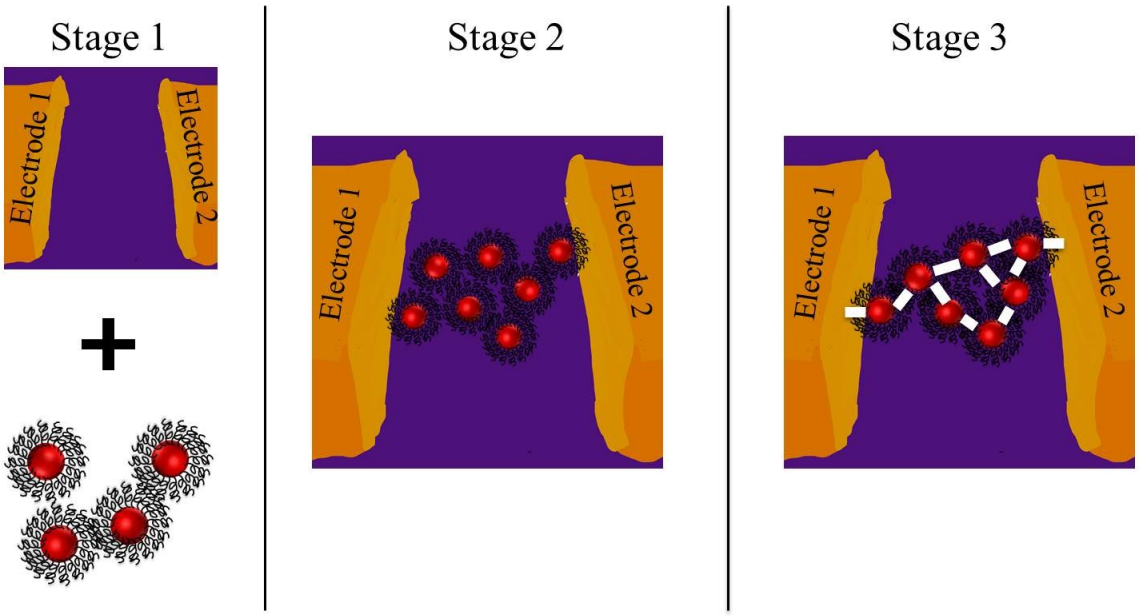

Schematic S1: Schematic diagram (not drawn to scale) describes the nanoMED at various stages of synthesis. At stage 1; nanogap is cut in approx. middle of thin gold line using focused beam of gallium ions and ω-thiol protected α,ω-octane dithiol coated gold nanoparticles (protected-AuNPs) are synthesized by wet chemistry. At Stage2; Protected-AuNPs are trapped in the gap by dielectrophoresis. Finally at stage 3, chemisorbed molecular junctions of biphenyl dithiol are created by molecular place exchange reaction. The nanoparticles act as interconnects between molecules and facilitate the bridging of the nanogap which is otherwise, an order of magnitude larger than length of the molecule.

2- Figure S1

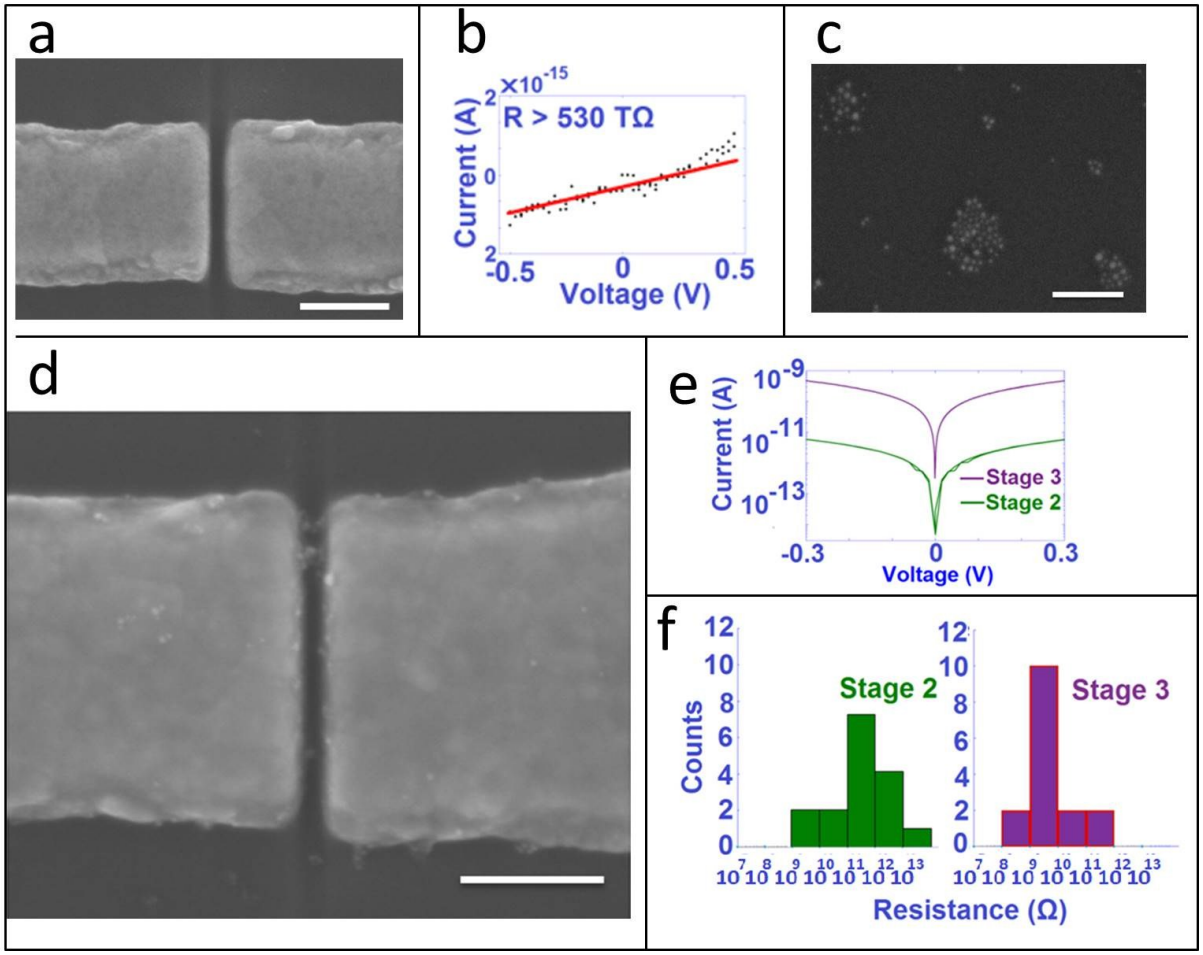

Figure S 1: Fabrication of nanoMED. (a-c-d) Scale bar is 100 nm. SEM images show an empty nanogap, protected-AuNPs and the nanogap which is bridged with protected-AuNPs. (a) An ≈20 nm wide gap made by FIB milling. (b) shows the empty gap resistance of more than 530 TΩ, calculated from the inverse-slope of the linear fitting (red line) of experimental data (black dots) between ±300 mV (c) Protected-AuNPs on Si/SiO_2 wafer. The size of the AuNPs is 4.9±1 nm. (d) Nano-device with few protected-AuNPs trapped in the nanogap by di-electrophoresis. (e) Semi log plots of current versus voltage showing the characteristic current conducted by the nano-device at different stages during the synthesis process i.e. (stage 2) Trapped nanogap and (Stage 3) after place exchange of protected-ODT with BPDT. (f) Comparison of the low bias resistance of devices fabricated for this work. Figure shows more than 2 orders of magnitude drop in resistance as devices move from stage 2 to stage 3 of synthesis.

3- Figure S2

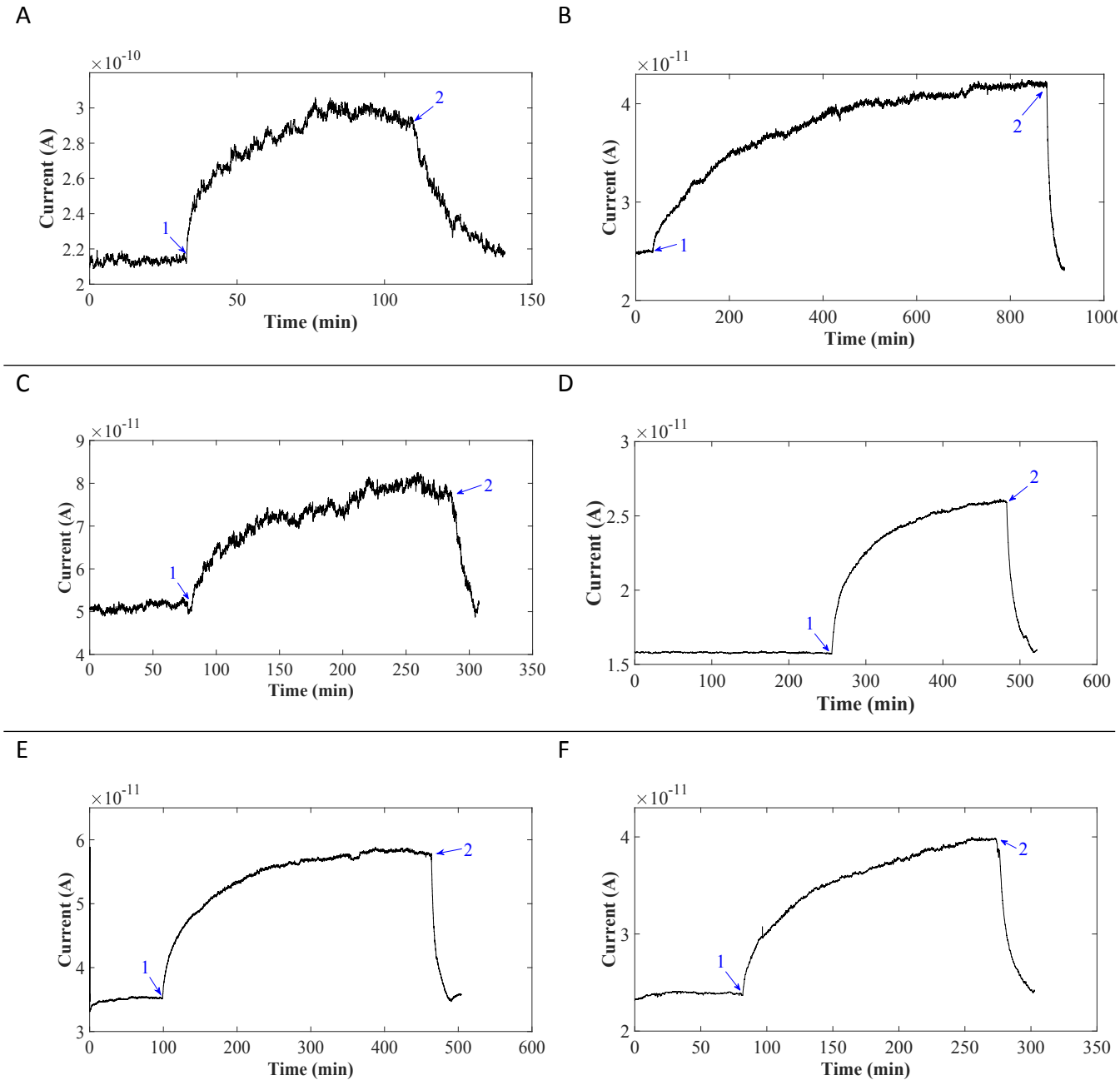

Figure S 2: Device at stage 3, response recorded for 100 ppm NO_2/ N_2 Exposure. NO_2 is injected at instant marked '1' and NO_2 is stopped and UV illumination is started at instances marked '2' in above figures.

4- Figure S3

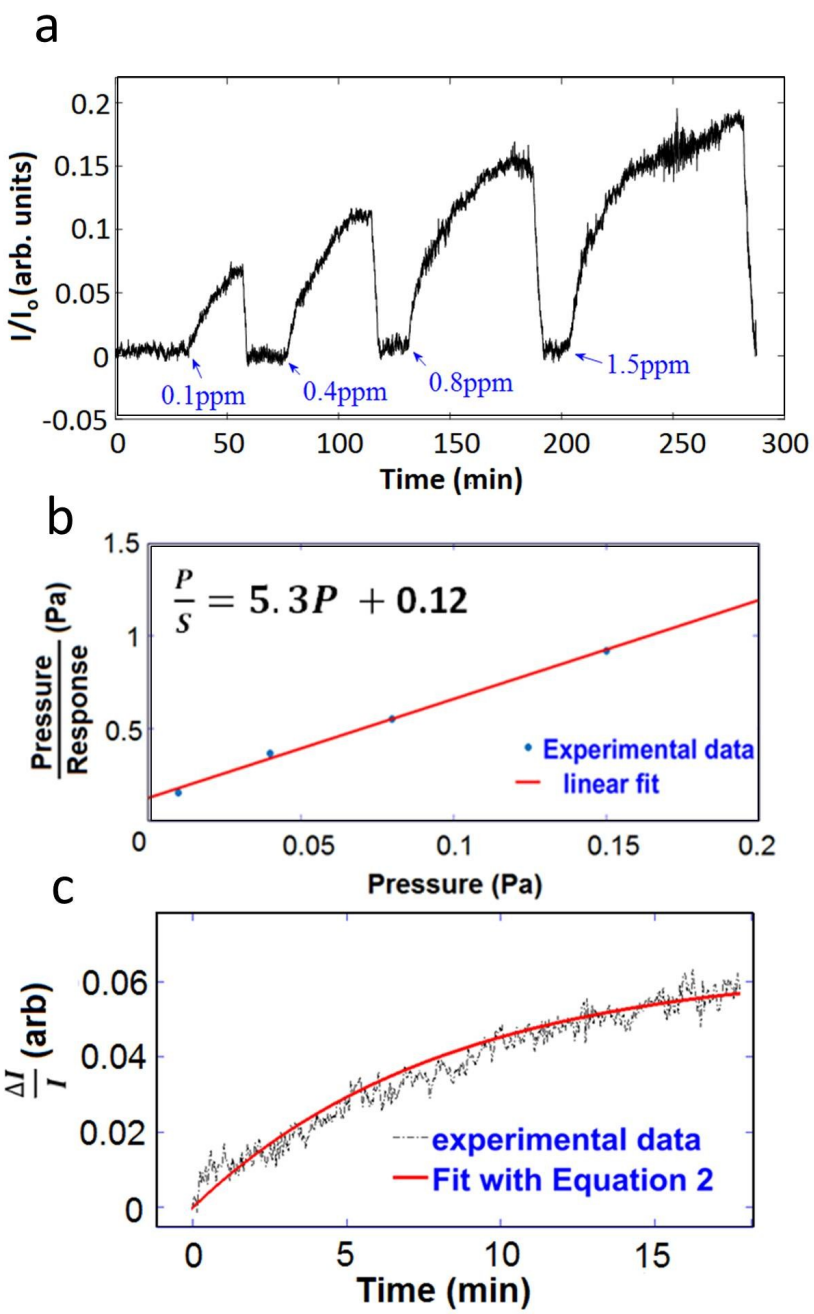

Figure S 3: (A) Dynamic response at an applied bias of V_B=150 mV and gas flow rate of 150 ml/min. Numbers with arrows are the ppm concentration of NO_2 in N_2. The device shows rising response with increased input concentrations of NO_2 in gas mixture. (B) Experimental data fitted with equation 1 to extract rate constant and maximum response. (C) Curve fitting with equation 2 to estimate adsorption rate constant.

5- Figure S4

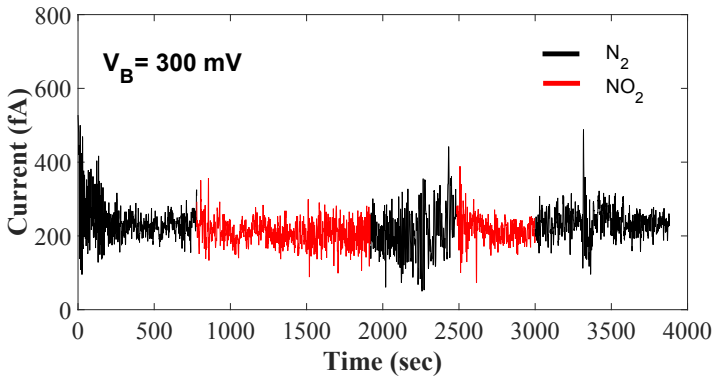

Figure S 4: Device at stage 2, does not show any change in average conducted current in N_2 as well as NO_2 exposure result

6- Figure S5

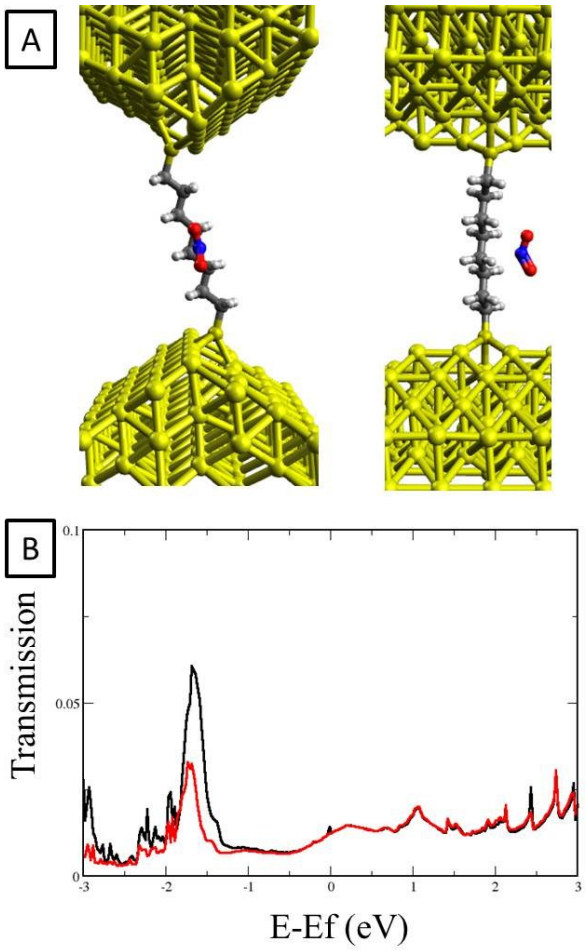

Figure S 5: (A)S-(CH_2)8-S between 11.93x12.66Å pieces of Au (110) surface with missing-row reconstruction, where S atoms are effectively connected close to the edge between two (111) facets(*15*); side and front view of configuration with NO_2 gas molecule. Right panel demonstrate slight bending away from NO_2 that results in effective stretching of alkene chain. (B) Transmission plot for system without (red line) and with NO_2 gas (black line). To reduce the computational time leads were computed with a single-ζ basis set used for Au with only 6s as the valence electron, providing accurate transmission in the range ±2eV